optica

Single-crystal diamond low-dissipation cavity optomechanics: supplementary material

MATTHEW MITCHELL[1,2], BEHZAD KHANALILOO[1,2], DAVID P. LAKE[1,2], TAMIKO MASUDA[1], J.P. HADDEN[1], AND PAUL E. BARCLAY[1,2,*]

[1] Department of Physics and Astronomy and Institute for Quantum Science and Technology, University of Calgary, Calgary, AB, T2N 1N4, Canada

[2] National Institute for Nanotechnology, Edmonton, AB, T6G 2M9, Canada

[*] Corresponding author: pbarclay@ucalgary.ca

Published 26 August 2016

This document provides supplementary information to "Single-crystal diamond low-dissipation cavity optomechanics," http://dx.doi.org/10.1364/optica.3.000963. First, we briefly describe the model used to extract the temperature shift of the cavity and finite element COMSOL simulations are used to predict the temperature increase observed in these devices. Secondly, we describe the model used to determine the laser detuning from cavity resonance for a bistable lineshape. We then discuss the calibration of the mechanical noise spectrum, which was utilized to determine the maximum oscillation amplitude as a function of input power. Lastly, we compare the $Q_m \cdot f_m$ product of our device to the current state of the art for optomechanical devices operating in ambient, vacuum, and cryogenic conditions, where we demonstrate the largest $Q_m \cdot f_m$ product to date in ambient conditions .

http://dx.doi.org/10.1364/optica.3.000963.s001

1. THERMAL SHIFT AND BISTABILITY

Here we outline the process for extracting the power dependent detuning, Δ. This process follows Carmon et al. [1], beginning with the expression for the shifted cavity resonance wavelength as a function of temperature, in thermal equilibrium

$$\lambda_o'(\Delta T) = \lambda_o + \Delta\lambda_o\,, \tag{S1}$$

$$= \lambda_o\left[1 + \left(\eta_\epsilon \epsilon + \eta_T \frac{1}{n}\frac{dn}{dT}\right)\Delta T\right]\,, \tag{S2}$$

$$= \lambda_o\left[1 + a\Delta T\right]. \tag{S3}$$

This expression is obtained by considering thermal expansion of the cavity, determined by the thermal expansion coefficient ϵ, and the thermo-optic effect, which shifts the refractive index n with temperature T. Here η_T and η_ϵ are geometric factors accounting for the optical mode overlap with the changing n and volume, respectively. Lumped constant a describes the net thermo-optic dispersion of the cavity mode. Using the room temperature single–crystal diamond values of $\epsilon \sim 1\times10^{-6}$ and $dn/dT \sim 1\times10^{-5}$ we can estimate the change in temperature of the cavity as

$$\Delta T = \left[\frac{\lambda_o'(\Delta T)}{\lambda_o} - 1\right]\cdot\frac{1}{a}. \tag{S4}$$

The shift of $\Delta\lambda_o \sim 400$ pm, as seen in Fig. 2(a) of the main text, corresponds to a change in device temperature $\Delta T \sim 50$ K. In this device the diamond forming the ~ 100 nm diameter pedestal has a significantly smaller thermal conductivity than that of bulk diamond (K $\sim 1500\,\mathrm{Wm^{-1}K^{-1}}$), reaching values $< 100\,\mathrm{Wm^{-1}K^{-1}}$ for nanowires < 100 nm in diameter [2]. In order to confirm that the cavity temperature shift predicted by Eq. (S4) was reasonable for our system we performed finite element COMSOL simulations to estimate ΔT, including the modified thermal conductivity for the pedestal, as shown in Fig. S1 for varying pedestal widths. Fig. S1 indicates that for a pedestal width of $\sim$ 100 nm, and corresponding diamond thermal conductivity of $\sim 300\,\mathrm{Wm^{-1}K^{-1}}$ a shift of 50 K is expected when $P_{abs} \sim 170\,\mu$W, where P_{abs} is the total power absorbed by the cavity. This corresponds to an optical absorption rate, $\gamma_{abs}\times 2\pi \sim 312$ MHz, which is $\sim 10\%$ of the total cavity decay rate, γ_{tot}. A linear relationship between ΔT and P_{abs} is observed for the pedestal thicknesses studied here.

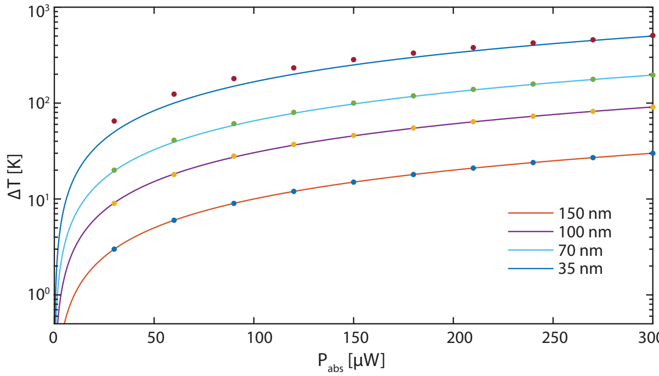

Fig. S1. Simulated change in temperature, ΔT of a $\sim$ 5 μm diameter microdisk as a function of absorbed power, P_{abs} for varying pedestal widths. Here the total heat flow to the device is given by P_{abs}/V, where V is the volume defined by the outer edge of the microdisk, with $V \sim 2\,\mu\mathrm{m}^3$. Each line represents a linear line of best fit to ΔT as a function of P_{abs}.

To convert (S3) to a form that depends on the experimentally measured, normalized cavity transmission $\overline{T}$, we treat the microdisk as being in thermal equilibrium with its environment such that

$$\dot{q}_{\mathrm{in}} = \frac{\gamma_{\mathrm{abs}}}{\gamma_{\mathrm{tot}}} P_d\,, \tag{S5}$$

where $\dot{q}_{\mathrm{in}}$, and P_d are the heat flow and power dropped into the cavity, respectively. Furthermore, we assume that

$$\dot{q}_{\mathrm{out}} = K\Delta\mathrm{T}\,, \tag{S6}$$

where K is the thermal conductivity between the cavity mode volume and the surrounding [1]. In thermal equilibrium the heat flow into the cavity will be equal to the heat flow out of the cavity, which allows us to write the equilibrium temperature as

$$\Delta\mathrm{T} = \frac{\gamma_{\mathrm{abs}}}{\gamma_{\mathrm{tot}}}\frac{P_d}{K}. \tag{S7}$$

Next we observe that since $P_d = (1-\overline{T})P_i$ where P_i is the fiber taper waveguide input power, we can write

$$\Delta\mathrm{T} = \frac{\gamma_{\mathrm{abs}}}{\gamma_{\mathrm{tot}}}\frac{(1-\overline{T})P_i}{K}\,, \tag{S8}$$

and the expected cavity mode shift in terms of the resonance contrast

$$\begin{aligned}
\lambda_{\mathrm{o}}'(\Delta\mathrm{T}) &= \lambda_{\mathrm{o}}\left[1 + a\Delta\mathrm{T}\right], && \text{(S9)}\\
&= \lambda_{\mathrm{o}}\left[1 + \left(\frac{a}{K}\frac{\gamma_{\mathrm{abs}}}{\gamma_{\mathrm{tot}}}P_i\right)(1-\overline{T})\right], && \text{(S10)}\\
&= \lambda_{\mathrm{o}}\left[1 + d(1-\overline{T})\right]. && \text{(S11)}
\end{aligned}$$

This gives the laser-cavity wavelength detuning, Δ_λ as

$$\begin{aligned}
\Delta_\lambda &= \lambda_{\mathrm{s}} - \lambda_{\mathrm{o}}'\,, && \text{(S12)}\\
&= \lambda_{\mathrm{s}} - \lambda_{\mathrm{o}} - d(1-\overline{T}). && \text{(S13)}
\end{aligned}$$

where $d = \frac{a}{K}\frac{\gamma_{abs}}{\gamma_{tot}}P_i$ is used as a free parameter in fitting our cavity transmission profile. The laser detuning Δ can then be calculated for any bistable lineshape.

2. SELF OSCILLATIONS AND DISPLACEMENT AMPLITUDE

In the weak damping regime ($\gamma_{\mathrm{m}} \ll \omega_{\mathrm{m}}$) the oscillation amplitude of a thermally driven harmonic oscillator is given by the equipartition theorem [3] as

$$x_{\mathrm{th}} = \sqrt{\frac{k_B \mathrm{T}}{m_{\mathrm{eff}}\omega_{\mathrm{m}}^2}}\,, \tag{S14}$$

where k_B is the Boltzmann constant, T = 295 K is the bath temperature, and $m_{\mathrm{eff}} = 40$ pg and $\omega_{\mathrm{m}}/2\pi \sim 2$ GHz are the effective mass and mechanical frequency of the radial breathing mode studied here, respectively. This results in $x_{\mathrm{th}} = 24$ fm and a zero point fluctuation motion, $x_{\mathrm{zpm}} = 0.32$ fm.

While $S_P(f) \propto \langle x^2\rangle$, where $\langle x^2\rangle$ is the variance of the mechanical displacement, one must be more careful when calculating the mechanical energy. Strictly speaking $\langle x^2\rangle$ is related to the single sided displacement spectral density $S_{xx}(\omega)$ by

$$\langle x^2\rangle = \int_0^\infty S_{xx}(\omega)\frac{d\omega}{2\pi}. \tag{S15}$$

This can be connected to the measured cavity transmission noise spectrum $S_P(\omega)$ through a cavity transfer function $H(\omega,\Delta)$, P_i, and g_{om} [4]

$$S_P(\omega) = g_{\mathrm{om}}^2 P_i^2 S_{xx}(\omega)H(\omega,\Delta). \tag{S16}$$

In this experiment we measure $S_P(\omega)$, and can compute the area under the curve, A, given by $A = \int_0^\infty S_P(\omega)\frac{d\omega}{2\pi}$. If we change P_i from P_{i_1} to P_{i_2}, keep Δ constant,and ignore the small ($\sim$ 0.02%) changes in ω_{m}, such that $H(\omega,\Delta;P_{i_1}) = H(\omega,\Delta;P_{i_2})$, we can show that the ratio of the area under the curve corresponding to P_{i_1} and P_{i_2} given by A_1 and A_2, respectively, is

$$\frac{A_1}{A_2} = \frac{P_{i_1}^2\langle x_1^2\rangle}{P_{i_2}^2\langle x_2^2\rangle}. \tag{S17}$$

We can then calibrate high P_i measurements to the thermal case, where P_i is small enough for optomechanical backaction effects to be ignored. The displacement amplitude, x_{om}, of the RBM in the self-oscillation regime can then be calculated as

$$x_{\mathrm{om}} = x_{\mathrm{th}}\sqrt{\frac{A_{\mathrm{om}}}{A_{\mathrm{th}}}\frac{P_T^2}{P_{\mathrm{om}}^2}}\,, \tag{S18}$$

where $\mathrm{A_{om}}$ and $\mathrm{A_{th}}$ are the area under the curve in the driven ($P_i = P_{\mathrm{om}}$) and thermal ($P_i = P_T$) states, respectively. Similarly, for the purpose of comparing mechanical spectra it is useful to calculate the normalized cavity transmission noise spectrum $\tilde{S}_P$, given by

$$\tilde{S}_P(\omega;P_i,\Delta) = S_P(\omega;P_i)\frac{P_i^2}{P_T^2}\bigg|_\Delta. \tag{S19}$$

The maximum oscillation amplitude x_{om} is shown as a function of dropped optical power in Fig. 3(a), where the absolute maximum oscillation amplitude was found to be $\sim$ 31 pm ($\sim x_{\mathrm{th}}\cdot 10^3$). Using finite element COMSOL simulations and by assuming that diamond behaves as a linear elastic material in the self oscillation regime, these amplitudes correspond to stress on the order of tens of MPa at the center of the microdisk.

3. COMPARISON OF $Q_M \cdot f_M$ PRODUCT

The device studied here demonstrates the largest $Q_m \cdot f_m$ product of an optomechanical device measured in ambient conditions to date. Figure S2 compares this value with a survey of some of the largest $Q_m \cdot f_m$ products observed in cavity optomechanical systems in ambient, cryogenic, and low pressure conditions. Note that higher $Q_m \cdot f_m$ products have been demonstrated compared to this work, but required either vacuum or low-temperature environments.

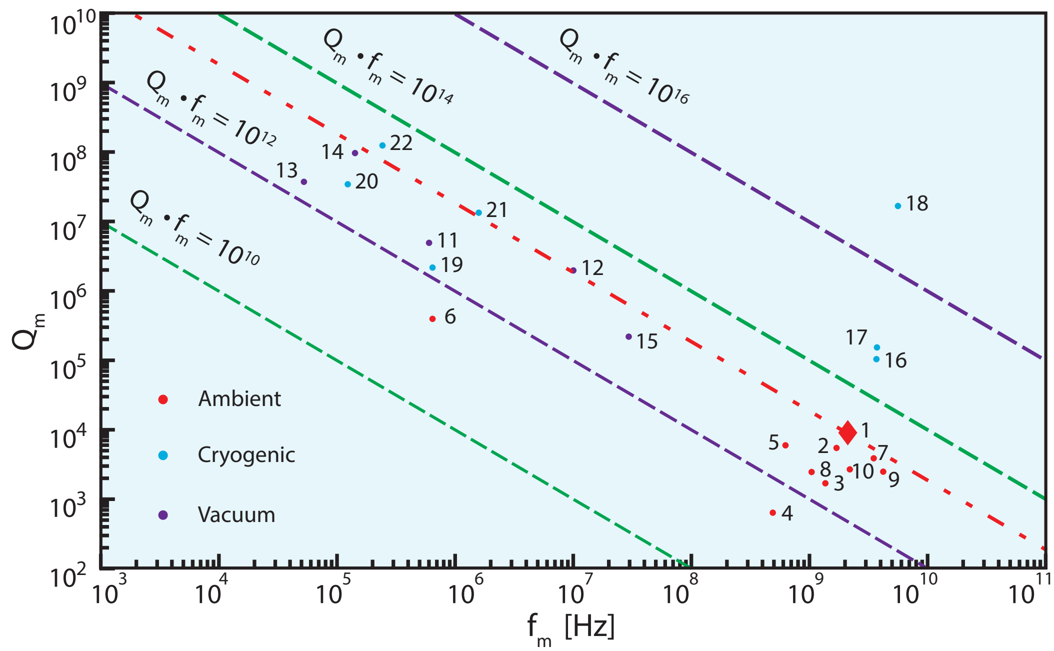

Fig. S2. Comparison of high $Q_m \cdot f_m$ product products for a variety of optomechanical systems, as listed in Table S1.

Table S1. Survey of highest $Q_m \cdot f_m$ products observed in cavity optomechanical systems to date, corresponding to those shown in Fig. S2.

No.	Author/Reference	Material	Structure
1	Mitchell et al. (This Work)	Diamond	Microdisk
2	Lu et al. [5]	SiC	Microdisk
3	Nguyen et al. [6]	GaAs	Microdisk
4	Mitchell et al. [7]	GaP	Microdisk
5	Liu et al. [8]	Si_3N_4	Microdisk
6	Fong et al. [9]	Si_3N_4	Beam & Waveguide
7	Grutter et al. [10]	Si_3N_4	Optomechanical Crystal
8	Xiong et al. [11]	AlN	Suspended Ring Resonator
9	Bochmann et al. [12]	AlN	Optomechanical Crystal
10	Eichenfield et al. [13]	Si	Optomechanical Crystal
11	Bui et al. [14]	Si_3N_4	Membrane Photonic Crystal + Fabry Pérot Cavity
12	Wilson et al. [15]	Si_3N_4	Membrane + Fabry Pérot Cavity
13	Reinhardt et al. [16]	Si_3N_4	Membrane + Fabry Pérot Cavity
14	Norte et al. [17]	Si_3N_4	Membrane Photonic Crystal + Fabry Pérot Cavity
15	Zhang et al. [18]	Si_3N_4	Tuning Fork + Microdisk
16	Chan et al.[19]	Si	Optomechanical Crystal + Phononic Shield
17	Krause et al. [20]	Si	Optomechanical Crystal + Phononic Shield
18	Meenehan et al. [21]	Si	Optomechanical Crystal + Phononic Shield
19	Fong et al. [9]	Si_3N_4	Beam + On-chip Interferometer
20	Yuan et al. [22]	Si_3N_4	Membrane + Superconducting Microwave Cavity
21	Purdy et al. [23]	Si_3N_4	Membrane + Fabry Pérot Cavity
22	Yuan et al. [24]	Si_3N_4	Membrane + Superconducting Microwave Cavity

REFERENCES

1. T. Carmon, L. Yang, and K. J. Vahala, "Dynamical thermal behavior and thermal self-stability of microcavities," Opt. Express **12**, 4742–4750 (2004).
2. W. Li, N. Mingo, L. Lindsay, D. A. Broido, D. A. Stewart, and N. A. Katcho, "Thermal conductivity of diamond nanowires from first principles," Phys. Rev. B **85**, 195436 (2012).
3. M. Aspelmeyer, T. J. Kippenberg, and F. Marquardt, "Cavity optomechanics," Rev. Mod. Phys. **86**, 1391–1452 (2014).
4. Q. Lin, J. Rosenberg, D. Chang, R. Camacho, M. Eichenfield, K. J. Vahala, and O. Painter, "Coherent mixing of mechanical excitations in nano-optomechanical structures," Nature Photon. **4**, 236–242 (2010).
5. X. Lu, J. Y. Lee, and Q. Lin, "High-frequency and high-quality silicon carbide optomechanical microresonators," Sci. Rep. **5**, 17005 (2015).
6. D. T. Nguyen, C. Baker, W. Hease, S. Sejil, P. Senellart, A. Lemaître, S. Ducci, G. Leo, and I. Favero, "Ultrahigh Q-frequency product for optomechanical disk resonators with a mechanical shield," Appl. Phys. Lett. **103**, 241112 (2013).
7. M. Mitchell, A. C. Hryciw, and P. E. Barclay, "Cavity optomechanics in gallium phosphide microdisks," Appl. Phys. Lett. **104**, 141104 (2014).
8. Y. Liu, M. Davanço, V. Aksyuk, and K. Srinivasan, "Electromagnetically induced transparency and wideband wavelength conversion in silicon nitride microdisk optomechanical resonators," Phys. Rev. Lett. **110**, 223603 (2013).
9. K. Y. Fong, W. H. P. Pernice, and H. X. Tang, "Frequency and phase noise of ultrahigh Q silicon nitride nanomechanical resonators," Phys. Rev. B **85**, 161410 (2012).
10. K. E. Grutter, M. I. Davanço, and K. Srinivasan, "Slot-mode optomechanical crystals: a versatile platform for multimode optomechanics," Optica **2**, 994–1001 (2015).
11. C. Xiong, X. Sun, K. Y. Fong, and H. X. Tang, "Integrated high frequency aluminum nitride optomechanical resonators," Appl. Phys. Lett. **100**, 171111–171111 (2012).
12. J. Bochmann, A. Vainsencher, D. D. Awschalom, and A. N. Cleland, "Nanomechanical coupling between microwave and optical photons," Nature Phys. **9**, 712–716 (2013).
13. M. Eichenfield, J. Chan, R. Camacho, K. Vahala, and O. Painter, "Optomechanical crystals," Nature **462**, 78–82 (2009).
14. C. H. Bui, J. Zheng, S. W. Hoch, L. Y. T. Lee, J. G. E. Harris, and C. Wei Wong, "High-reflectivity, high-Q micromechanical membranes via guided resonances for enhanced optomechanical coupling," Appl. Phys. Lett. **100**, 021110 (2012).
15. D. J. Wilson, C. A. Regal, S. B. Papp, and H. J. Kimble, "Cavity optomechanics with stoichiometric SiN films," Phys. Rev. Lett. **103**, 207204 (2009).
16. C. Reinhardt, T. Müller, A. Bourassa, and J. C. Sankey, "Ultralow-noise SiN trampoline resonators for sensing and optomechanics," arXiv:1511.01769 (2016).
17. R. A. Norte, J. P. Moura, and S. Gröblacher, "Mechanical resonators for quantum optomechanics experiments at room temperature," Phys. Rev. Lett. **116**, 147202 (2016).
18. R. Zhang, C. Ti, M. I. Davanço, Y. Ren, V. Aksyuk, Y. Liu, and K. Srinivasan, "Integrated tuning fork nanocavity optomechanical transducers with high $f_M Q_M$ product and stress-engineered frequency tuning," Appl. Phys. Lett. **107**, 131110 (2015).
19. J. Chan, T. P. M. Alegre, A. H. Safavi-Naeini, J. T. Hill, A. Krause, S. Groblacher, M. Aspelmeyer, and O. Painter, "Laser cooling of a nanomechanical oscillator into its quantum ground state," Nature **478**, 89–92 (2011).
20. A. G. Krause, J. T. Hill, M. Ludwig, A. H. Safavi-Naeini, J. Chan, F. Marquardt, and O. Painter, "Nonlinear radiation pressure dynamics in an optomechanical crystal," Phys. Rev. Lett. **115**, 233601 (2015).
21. S. M. Meenehan, J. D. Cohen, G. S. MacCabe, F. Marsili, M. D. Shaw, and O. Painter, "Pulsed excitation dynamics of an optomechanical crystal resonator near its quantum ground state of motion," Phys. Rev. X **5**, 041002 (2015).
22. M. Yuan, V. Singh, Y. M. Blanter, and G. A. Steele, "Large cooperativity and microkelvin cooling with a three-dimensional optomechanical cavity," Nat. Commun. **6** (2015).
23. T. P. Purdy, R. W. Peterson, P.-L. Yu, and C. A. Regal, "Cavity optomechanics with Si_3N_4 membranes at cryogenic temperatures," New J. Phys. **14**, 115021 (2012).
24. M. Yuan, M. A. Cohen, and G. A. Steele, "Silicon nitride membrane resonators at millikelvin temperatures with quality factors exceeding 10^8," Appl. Phys. Lett. **107**, 263501 (2015).